J Mater Sci: Mater Electron (2017) 28:12747–12754
DOI 10.1007/s10854-017-7100-6

One-step hydrothermal synthesis of Ni_3S_4@MoS_2 nanosheet on carbon fiber paper as a binder-free anode for supercapacitor

Feng Huang[1] · Aihua Yan[1] · Yanwei Sui[1] · Fuxiang Wei[1] · Jiqiu Qi[1] · Qingkun Meng[1] · Yezeng He[1]

Received: 3 March 2017 / Accepted: 6 May 2017 / Published online: 11 May 2017

Abstract Ni_3S_4@MoS_2 nanosheets grown on the carbon fiber paper (Ni_3S_4@MoS_2/CFP) were successfully prepared via a facile one-step hydrothermal technique. Serving as a supercapacitor electrode, the obtaining Ni_3S_4@MoS_2/CFP exhibits a remarkable specific capacitance of 1296 F/g, high rate capability of 57.8%, and excellent cycling stability of 96.2% retention after 5000 cycles. The superior electrochemical properties of Ni_3S_4@MoS_2/CFP nanocomposite is attributed to the synergistic effects of the layeredNi_3S_4, MoS_2 and the conductive CFP.

1 Introduction

As one of the most promising energy storage devices, supercapacitor (SC), also named electrochemical capacitor, has attracted worldwide attention due to its excellent properties, such as rapid recharge ability, high power density, long-life cycles, eco-friendly nature and low-cost preparation [1–3]. Based on the different charge storage mechanism, supercapacitor is normally divided two different categories: double-layer capacitor and pseudo-capacitor. The former usually uses carbon material as electrode material [4–7], while the latter employs some metal oxide and conducting polymers as electrode material based on redox capacitive mechanism [8–11]. The continuous exploration of high-capacity materials and the design of optimal electrode architecture have been an indispensable part of the significant development of SC.

Metal sulfide has recently aroused the attention due to their unique electrochemical property [12–14]. As a typical example, molybdenum sulfide (MoS_2)where Mo atom can easily prompt redox faradaic reaction in the interlayer space due to the oxidation states from the +2 to +6 has been proved to be an promising electrode material and its theoretical specific capacitance is high up to 1000 F/g [15, 16]. Ramadoss et al. prepared mesoporous MoS_2 nanostructure by a hydrothermal method and obtained maximum capacitance of 376 and 403 F/g at a scan rate of 1 mV/s in 1 M Na_2SO_4 and KCl electrolyte solutions respectively [17]. Wang et al. have synthesized a hierarchical MoS_2 nanospheres by hydrothermal method for supercapacitors, with their capacitance of 142 F/g at current density of 0.59 A/g [18]. However, the specific capacitance of MoS_2 is still very poor due to low electronic conductivity and small quantities of accessible active sites of MoS_2, which limited the further application and development.

On the other hand, another transition metal sulfide, nickel sulfides, have many advantages for the application of supercapacitors because of good inductivity, natural abundance and versatility [13, 19–21]. Wang et al. adopted hydrothermal synthesis to prepare rigid three-dimensional Ni_3S_4 nanosheet frames with a specific capacitance of 1213 F/g and capacitance retention around 60% after 2000 cycles [22]. Zhang et al. have prepared hierarchical structure Ni_3S_2 (710.4 F/g and 84% cycling retention after 2000 cycles) [23]. Yang et al. have synthesized a hierarchical flower-like β-NiS electrode, which show high performance 857.76 F/g and 44% retention after 1000 cycles [24]. Although these nickel sulfides show very high specific capacitance, the cycle stability is poor.

✉ Yezeng He
hyz0217@hotmail.com

[1] School of Materials Science and Engineering, China University of Mining and Technology, Xuzhou 221116, People's Republic of China

In this work, we synthesized a novel Ni_3S_4@MoS_2 nanocomposite grown on carbon fiber paper (CFP) with excellent electric conductivity and larger specific surface via facile one-step hydrothermal technique. TheNi_3S_4@MoS_2/CFP electrode shows a high specific performance of 1296 F/g at 1 A/g in 2 M KOH solution. In addition, the Ni_3S_4@MoS_2/CFP electrode showed excellent cyclic stability (retention 96.2% after 5000 cycles at 5 A/g) and high rate capability. When the current density increase from 1 to 10 A/g, the specific capacitance retention of Ni_3S_4@MoS_2/CFP can maintain 57.8%.

2 Experimental section

2.1 Material

All the reagents used in this experiment were of analytical grade and used without purification. Thiourea (NH_2CSNH_2), Sodium molybdatedihydrate ($Na_2MoO_4{\cdot}2H_2O$), nickel(II) chloride hexahydrate ($NiCl_2{\cdot}6H_2O$) and Anhydrous ethanol (C_2H_6O) were purchased from Aladdin Industrial Corporation. Carbon fiber paper (CFP) (product of Toray, Japan; Teflon treated: 5% wt. wet proofing; thickness: 0.11 mm), used as working electrode, was obtained from Fuel Cell Store, USA. The water was purified through a Lab Pure Water System (18.25 mΩ).

2.2 Synthesis of Ni3S4@MoS2/CFP

Before the synthesis, the CFP was hydrothermally pretreated with 0.1 M nitric acid (HNO_3) in 9 °C for 5 h and subsequently rinsed with deionized water and absolute ethanol. Finally, the CFP was dried at 70 °C in vacuum for 6 h then the mass of CFP was measured by using balance. Typically, the Ni_3S_4@MoS_2/CFP nanocomposite was prepared through a facile solvothermal method. Initially, 1.25 mmol $Ni(Cl)_2{\cdot}6H_2O$, 2.5 mmol $Na_2MoO_4{\cdot}2H_2O$ and 6.25 mmol NH_2CSNH_2 were dissolved in a 30 ml mixed solution of DI water and anhydrous ethanol (1:1 in volume).Then, two pieces of carbon fiber paper (1×2 cm^2) vertically insert into the Teflon holder were subsequently soaked in the solution, and the precursor solution was magnetically stirred by ultrasonication for 0.5 h following by heated the solution to 180 °C in an electric oven, and kept at that temperature for 48 h. After natural cooling to room temperature, the as synthesized electrodes were then taken out, ultrasonically cleaned for 5 min in the DI water and rinsed with ethanol several times, dried in vacuum at 70 °C over night. The mass loading of Ni_3S_4@MoS_2/CFP nanosheets on carbon fiber paper was 0.5 mg/cm^2. For properties comparison, pristine MoS_2/CFP and Ni_3S_4/CFP were prepared to follow the similar procedure in the absence of $Ni(Cl)_2{\cdot}6H_2O$ and $Na_2MoO_4{\cdot}2H_2O$, respectively.

2.3 Characterization

The MoS_2/CFP, Ni_3S_4/CFP and Ni_3S_4@MoS_2/CFP sample were characterized for structural properties using X-ray diffraction (D8 Advance, Bruker, Germany) with Cu-Kα radiation from 10°–80°with scan rate of 8°/min. The morphology and structure of the products were observed by field emission SEM (Hitachchi SU-8000) equipped with high-resolution TEM (HRTEM, Tecnai G2F20).

2.4 Electrochemical measurements

Electrochemical measurements were performed on a CHI660D (Chenhua, shanghai, China) electrochemical working station in 2 M KOH aqueous electrolyte solution under three electrode systems consisted of a working electrode, a platinum plate counter electrode, and a saturated calomel electrode (SCE) reference electrode at room temperature. Cyclic voltammetry (CV), galvanostatic charge–discharge curves, and electrochemical impedance spectroscopy (EIS) were conducted in 2 mol/L KOH electrolyte with typical three-electrode cells (Pt as the counter electrode, Ag/AgCl as the reference electrode, and Ni_3S_4@MoS_2/CFP as the working electrode). CV curves were collected over a voltage range from 0 to 0.5 V, and galvanostatic charge–discharge curves were measured over a voltage range from 0 to 0.44 V. The specific capacitance can be calculated from the galvanostatic charge–discharge curve according to Eq. (1)

$$C = \frac{I\Delta t}{m\Delta v} \tag{1}$$

where C is the specific capacitance, I is the current, Δt is the discharge time, Δv is the potential window, and m is mass of the electroactive material. EIS was recorded in the frequency range from 0.01 to 100 kHz at an open-circuit potential.

3 Results and discussion

The Ni_3S_4@MoS_2/CFP nanostructure was successfully prepared through a facile and low temperature hydrothermal method. The fabrication of Ni_3S_4@MoS_2/CFP nanostructures is schematically depicted in Fig. 1. During the reaction, the chemical reaction occurred at the surface of the cleaned carbon fiber pager, and the active species (S ions) will be released from NH_2CSNH_2 according Eq. (2). At last the S ions with MoO_4^{2-} and Ni^{2+} ions to produce Ni_3S_4@MoS_2.

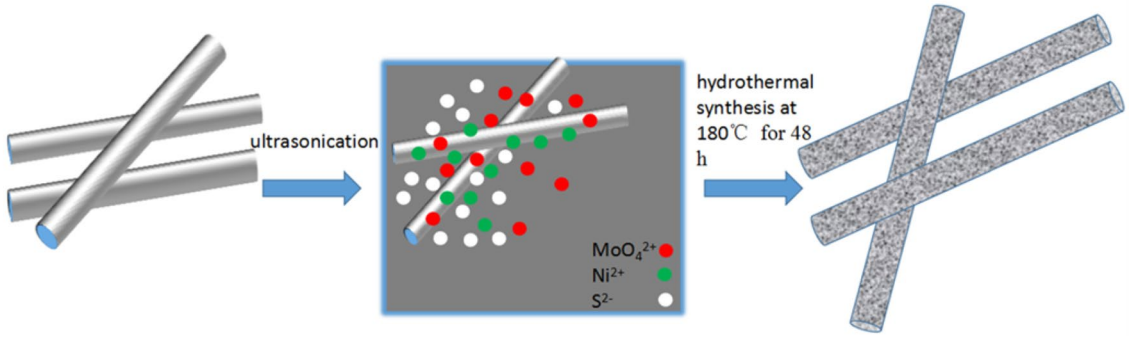

Fig. 1 Schematic the reaction process of the Ni_3S_4@MoS_2/CFP

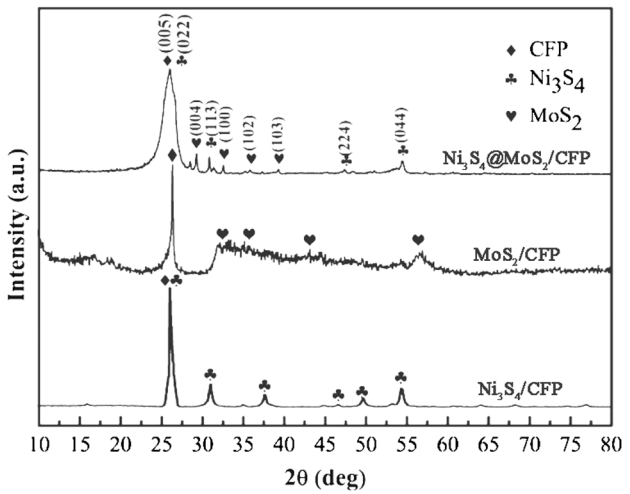

Fig. 2 XRD patterns ofNi_3S_4@MoS_2/CFP, MoS_2/CFP and Ni_3S_4/CFP, respectively

$$NH_2CSNH_2 + H_2O \rightarrow 2NH_3 + 2H_2S + CO_2 \quad (2)$$

The composition and purity of the as-obtained samples are analyzed by XRD technique. Figure 2 displays the XRD pattern of MoS_2, Ni_3S_4 and Ni_3S_4@MoS_2 loaded on the CFP, respectively. The typical diffraction peak around 26.6° of all pattern arise from the CFP substrate (JCPDS card no. 26-1080).From the XRD pattern of Ni_3S_4@MoS_2/CFP, the diffraction peaks located at 2θ = 26.5°, 31.8°, 47.3°and 54.8° can be perfectly indexed to (022), (113), (224) and (044) planes of Ni_3S_4 (JCPDS card no. 43-1469), which is agreed with those of Ni_3S_4/CFP. For MoS_2, the curve of Ni_3S_4@MoS_2 shows serious sharp peaks at 29.2°, 32.6°, 35.8°and 39.5°which could be ascribed to the (004), (100), (102) and (103) phase of hexagonal MoS_2 (JCPDS 37-1942) in accordance with MoS2/CFP, respectively. In addition, no obvious peak of (002) diffraction peak in the MoS_2/CFP, Ni_3S_4@MoS_2/CFP are attributed to the low crystal of MoS_2 [25].

The morphological studies of the MoS_2/CFP, Ni_3S_4/CFP andNi_3S_4@MoS_2/CFP were carried out by electron microscopy techniques. Figure 3 displays the surface morphology after the MoS_2/CFP, Ni_3S_4/CFP andNi_3S_4@MoS_2composite deposition on CFP. Figure 3b shows that MoS_2 flower-like sheets uniformly covered on the surface of the CFP. As shown in Fig. 3c, the pristine Ni_3S_4nanospherescompactlyaggregated on surface of CFP with size of 100–300 nm. However, it can be observed that numerous Ni_3S_4 nanoparticles are homogeneously distributed on the surface of MoS_2 the Fig. 3d. In addition, Fig. 3e, f indicate that the morphology of Ni_3S_4changes from compact sphere to cluster. During the reaction, the MoS_2 layers have severely affected nuclei formation and crystal growth of Ni_3S_4 nanoparticles. The highly magnified SEM image in Fig. 3f shows that the Ni_3S_4@$MoS_2$is composed of cluster with the size of 100–150 nm by piling up intertwined sheet-like structure. The flower-like sheets MoS_2 might provide more efficient contacts between active material and electrolyte. But the poor conductivity of MoS_2 might limit charge transition. In this case, the conductive Ni_3S_4 nanoparticles could efficiently lower the internal resistance and provide perfect continuous channels for electron transportation.

More details of the morphological and structural features of as-obtained Ni_3S_4@MoS_2 separated from the CFP by ulrasonication are studied by TEM technique. Figure 4 shows the TEM images of the synthesized Ni_3S_4@MoS_2 nanocomposite which is composed of many nanosheets. The result is consistent with what has been indicated by the SEM pattern in Fig. 3d–f. As shown in Fig. 4a, b, the Ni_3S_4@MoS_2 display a morphology of folded and tangled layers with some folded edges exhibiting parallel lines corresponding to the different layers of MoS_2 sheets. In Fig. 4c, d, the high-resolution TEM (HRTEM) images of Ni_3S_4@MoS_2indicate that the interlayer spacing ofNi_3S_4 sheets is 0.29 nm and interplanar spacing of the MoS_2 in the composite is 0.62 nm, which

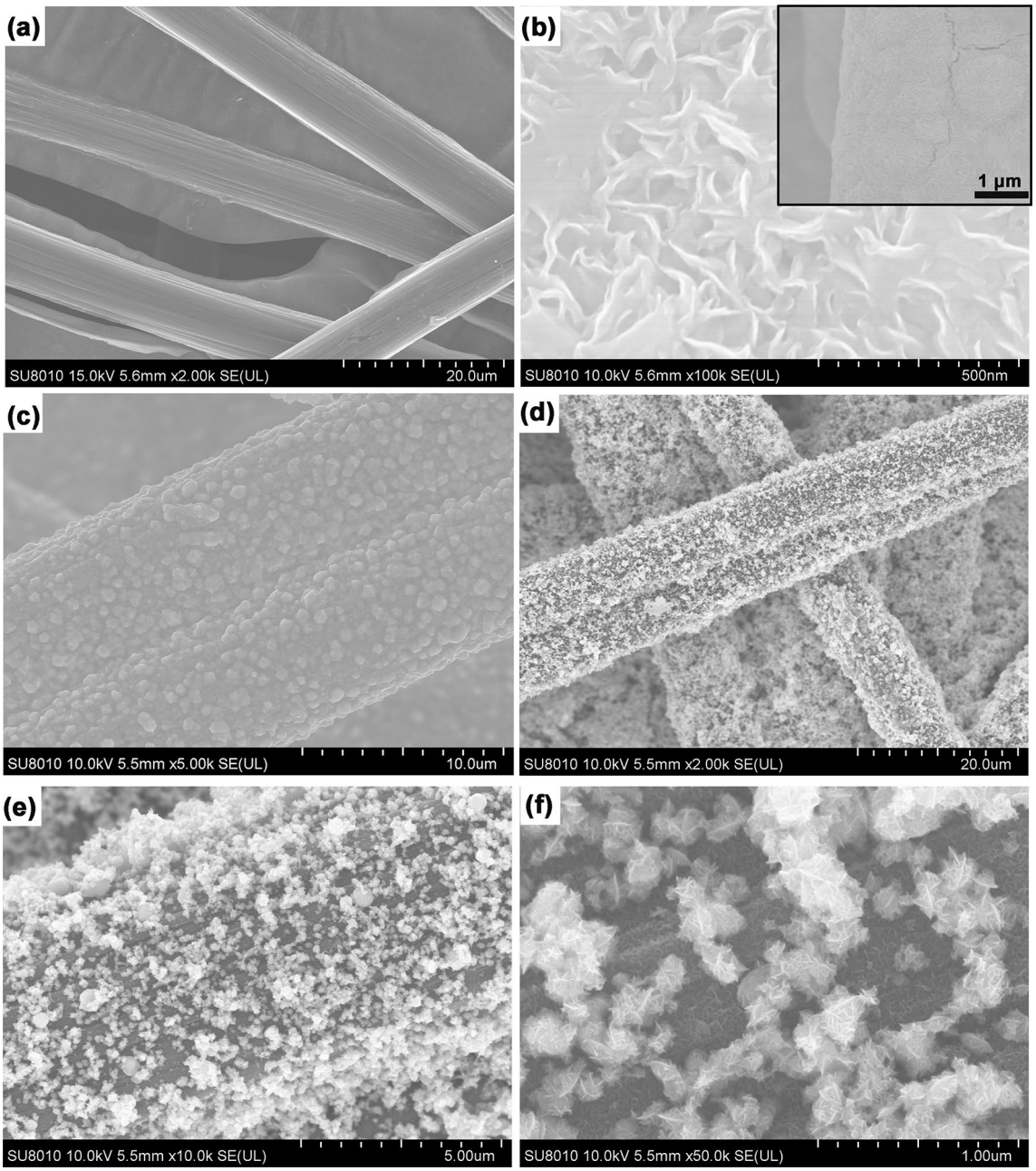

Fig. 3 SEM images of **a** pure CFP, **b** MoS_2/CFP, **c** Ni_3S_4/CFP, **d–f** Ni_3S_4@MoS_2/CFP

match well with the (113) plane of Ni_3S_4 and (002) plane of MoS_2, respectively [22, 25].

The electrochemical performances of the as-prepared MoS_2/CFP,Ni_3S_4/CFP and Ni_3S_4@MoS_2/CFP nanocomposite were carried out in a three electrode system in 2 M KOH aqueous solution as shown in Fig. 5a. Clearly, Ni_3S_4@MoS_2/CFP has larger area CV curves than that of the MoS_2/CFP and Ni_3S_4/CFP, which suggests the higher capacitive capability of theNi_3S_4@MoS_2/CFP. In addition, the peaks at 0.35 and 0.21 V of Ni_3S_4@MoS_2/CFP are too strong compared with bare MoS_2/CFP. This is the main reason why theNi_3S_4@MoS_2/CFP nanocomposite only exhibits one pair of redox peaks. The appearance of a pair of remarkable redox peaks indicates the nanosheets of Ni_3S_4@MoS_2/CFP offering more active sites for redox charge transfer. For the curves of Ni_3S_4@MoS_2/CFP composite, the observed characteristic oxidation and reduction position (oxidation peak around +0.35 V and reduction peak around +0.21 V) exhibited in the CV curves are related to faradic redox reactions reacting at the Ni_3S_4@MoS_2/CFP surface

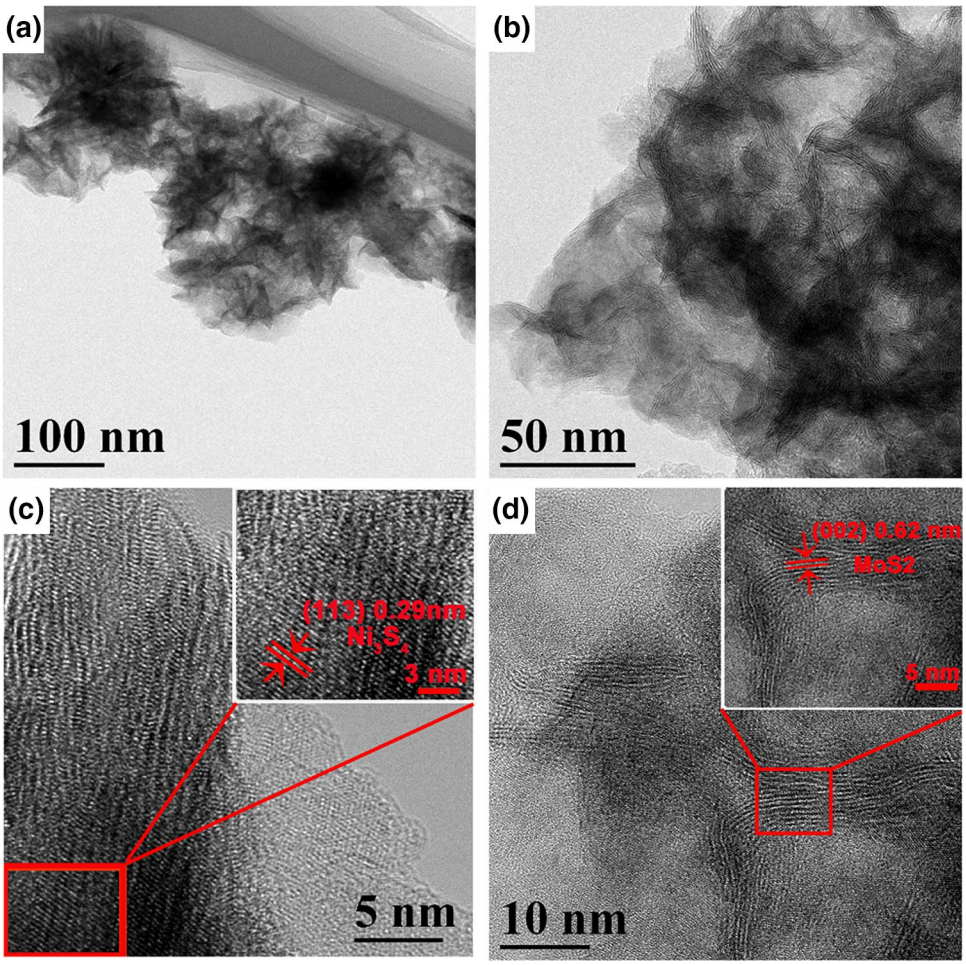

Fig. 4 **a, b** TEM and **c, d** HRTEM and the images of Ni_3S_4 and MoS_2 (*inset*), respectively

in alkaline KOH electrolyte [17, 26–28]. The main reaction mechanism can be described as follows,

$$NiS_x + 4OH^- - 2e^- \rightarrow NiO_2 + S_x^{2-} + 2H_2O$$

$$NiO_2 + H_2O + e^- \leftrightarrow NiOOH + OH^-$$

$$NiOOH + H_2O + e^- \leftrightarrow Ni(OH)_2 + OH^-$$

$$MoS_2 + K^+ + e^- \leftrightarrow MoS - SK^+$$

Figure 5b illustrates the charge–discharge curves ofMoS_2/CFP, Ni_3S_4/CFP and Ni_3S_4@MoS_2/CFP in the potential range of 0–0.44 V at a current density of 1 A/g Ni_3S_4@MoS_2/CFP nanocomposite shows the best charge storage properties, compared to MoS_2/CFP and Ni_3S_4/CFP. The specific capacitances of the prepared Ni_3S_4@MoS_2/CFP were calculated to be 1296 F/g lager than those of MoS_2/CFP (150 F/g) and Ni_3S_4/CFP (364 F/g) at 1 A/g. These results are in good accordance with the CV curves. Figure 5c shows the CV curves of the Ni_3S_4@MoS_2/CFP composite at a san rate of 5–30 mV/s in the potential window of 0.0–0.5 V versus SCE in 2 M KOH. The CV curves of three electrodes show an obvious redox but rectangular shape, which indicate that electrodes at certain scan rate possess a typical redox capacitive mechanisms pseudocapacitance. It is obvious that the integrated area gradually increased and the shape of CV curves remained similar, implying good rate capability.Moreover, the current density increases and the oxidation peak shifts to a more positive position, while the reduction peak shifts to a more negative position. This is due to the increased internal resistance within the pseudoactive material with the increase in scan rate.For comparison, the CV of the pristine CFP and Ni_3S_4@MoS_2/CFP at 5 mV/s are also shown in Fig. 5d. It is noted that the CFP is of almost no electrochemical performance. The supercapacitive characteristic can also be measured by constant current charge–discharge cycling test. Figure 5c shows the galvanostatic charge–discharge curves of atNi_3S_4@MoS_2/CFP at current densities of 1–10 A/g with a platform during process of charge and discharge, respectively, corresponding to a pair of redox peaks in CV curves. The specific capacitance can be calculated by Eq. (1). The calculated results indicate the specific capacitances of the material are 1296, 936, 893, 863, 829, 763 and 750 F/g at

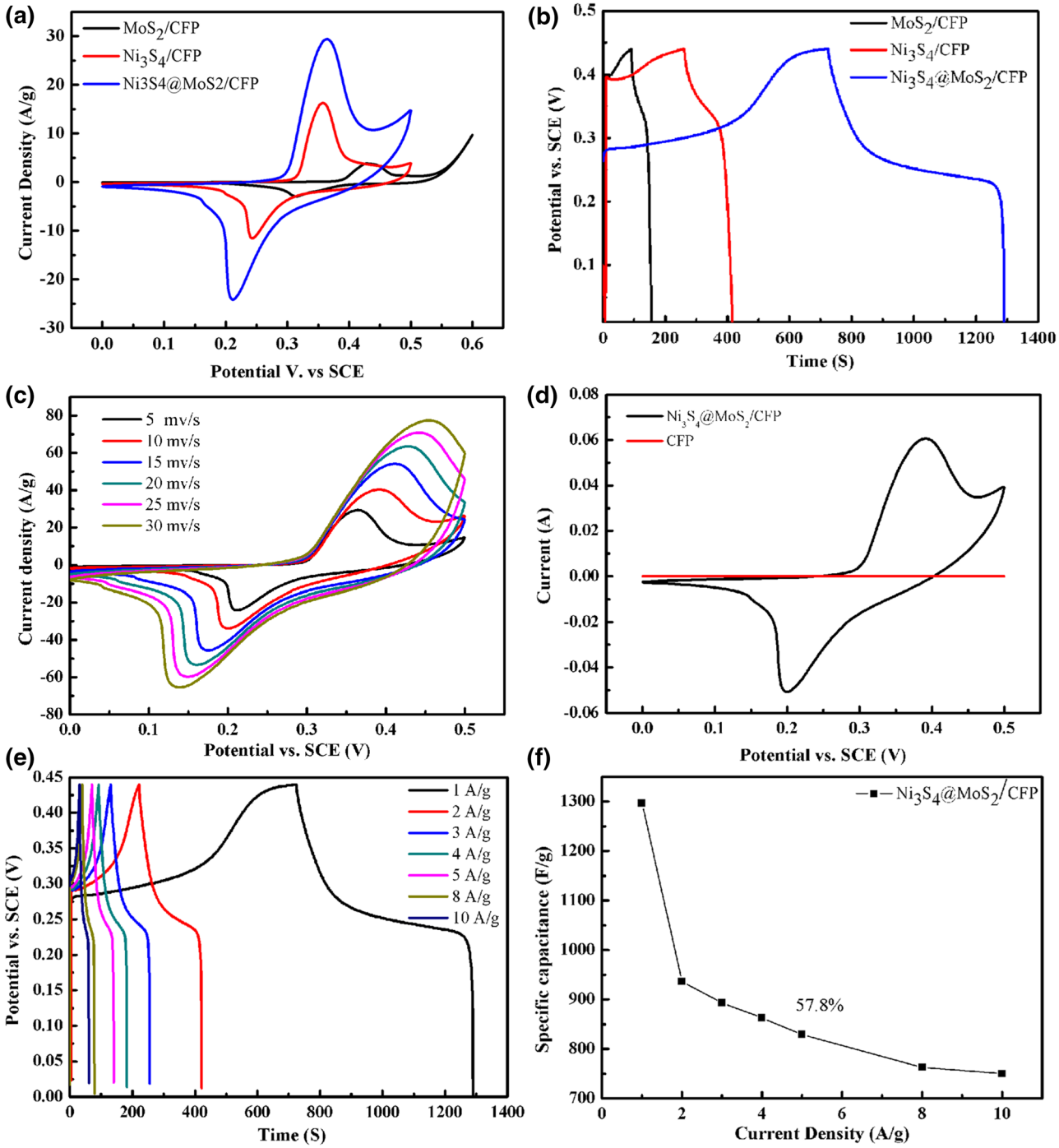

Fig. 5 **a** Cyclic voltammograms curves of MoS_2/CFP, Ni_3S_4/CFP and Ni_3S_4@MoS_2/CFPat scan rate of 5 mV/s, respectively; **b** galvanostatic charging/discharging curves of MoS_2/CFP, Ni_3S_4/CFP and Ni_3S_4@MoS_2/CFP at current density of 1 A/g, respectively; **c** cyclic voltammograms curves of Ni_3S_4@MoS_2/CFP at different scan rate in 2 M KOH; **d** CV curves of Ni_3S_4@MoS_2/CFP and CFPat scan rate of 5 mV/s, respectively; **e** galvanostatic charging/discharging curves at a serious current densities for Ni_3S_4@MoS_2/CFP in 2 M KOH; **f** rate capability curves of Ni_3S_4@MoS_2/CFP at various current density

current densities of 1, 2, 3, 4, 5, 8 and 10 A/g respectively, which is better than that of pristine Ni_3S_4reported elsewhere [22]. The large specific capacitance can be attributed to unique sheet structure. Furthermore, Fig. 5d exhibits the Ni_3S_4@MoS_2/CFP electrodes as a function of current density. It indicates that the specific capacitance decreases with the increase of current density. However, the specific capacitance retention of Ni_3S_4@MoS_2/CFP can maintain

57.8% when the current density increase from 1 to 10 A/g, which suggests that efficient surface redox reaction take place on the Ni_3S_4@MoS_2/CFP. The results indicate that the Ni_3S_4@MoS_2/CFP composite could be recognized as one of the important potential electrode material in application of electrodes and batteries.

The cycle stability of Ni_3S_4@MoS_2/CFP composite was evaluated by repeating the constant current charge/discharge test in a potential window of 0–0.44 V (vs. SCE) at a current density 5 A/g for 5000 cycles. Figure 6a shows that the specific capacitance has been increased during the first 1000 cycles, mainly due to the electrode material activated during the continuing charge–discharge process. Finally, the capacitance retention of Ni_3S_4@MoS_2/CFP in 2 M KOH electrolytes remains around 96.2% after 5000 cycles. EIS is one of the prominent tools to understand the charge-transfer behavior and capacitive nature of an electrode–electrolyte interface system with respect to the applied frequency [29]. Figure 6b shows Nyquist plots for the Ni_3S_4@MoS_2/CFP electrode with a parallel model before and after 5000 cycles. In the high-frequency region, the first intercept of the semicircle with the real axis corresponds to the intrinsic ohmic resistance of an equivalent series resistance (Rs) of the electrolyte and electrode. Obviously, the Rs of Ni_3S_4@MoS_2/CFP electrodes was measured to be 0.7718 and 0.611 Ω, respectively. Then, the semicircle in the high-medium frequency region is attributed to the charge-transfer impedance (Rct) at the electrode and electrolyte interface. The value of Rct is measured as semicircular arc diameter .Therefore, the Rct of Ni_3S_4@MoS_2/CFP electrodes increased from 2.32 to 3.88 Ω after the 5000 cycles. In the low frequency region, the straight line in the low frequency range is related to the diffusive resistance of the electrolyte into interior of the electrode and the ion diffusion in to the electrode, suggesting the ideal capacitive behavior of the Ni_3S_4@MoS_2/CFP. The high performance of the hybrid composite electrodes is attributed to the following some advantages of the electrode. (1) Carbon fiber paper (CFP), a network of micro-sized carbon fibers, has many excellent characteristics such as large surface area, high porosity, good electric conductivity, and excellent chemical stability in a wide variety of liquid electrolytes; (2) Ni_3S_4@MoS_2/CFP accumulate to form pores for ion-buffering reservoirs to improve the diffusion rate of ions; (3) the conductive Ni_3S_4 could efficiently lower the internal resistance; (4) the sheeted Ni_3S_4@MoS_2/CFP offer large surface area with short electrons and ions diffusion path and the unique structure of Ni_3S_4@MoS_2increase the amount of electroactive sites for the effective utilization of Ni_3S_4@MoS_2 active material.

4 Conclusion

In summary, Ni_3S_4@MoS_2 nanosheets grown on the carbon fiber paper (Ni_3S_4@MoS_2/CFP) composites were successfully prepared via a facile one-step hydrothermal technique. The specific capacitance of Ni_3S_4@MoS_2/CFP nanocomposite has been measured to be 1296 F/g at a discharge density of 1 A/g. the specific capacitance retention of Ni_3S_4@MoS_2/CFP can maintain 57.8% with the current densities from 1 to 10 A/g. Furthermore, the Ni_3S_4@MoS_2/CFP nanocomposite displays an excellent long-time cycling stability, retaining 96.2% of the initial capacitance after 5000 cycles at current density of 5 A/g. These excellent results indicate that the Ni_3S_4@MoS_2/CFP nanocomposite is a

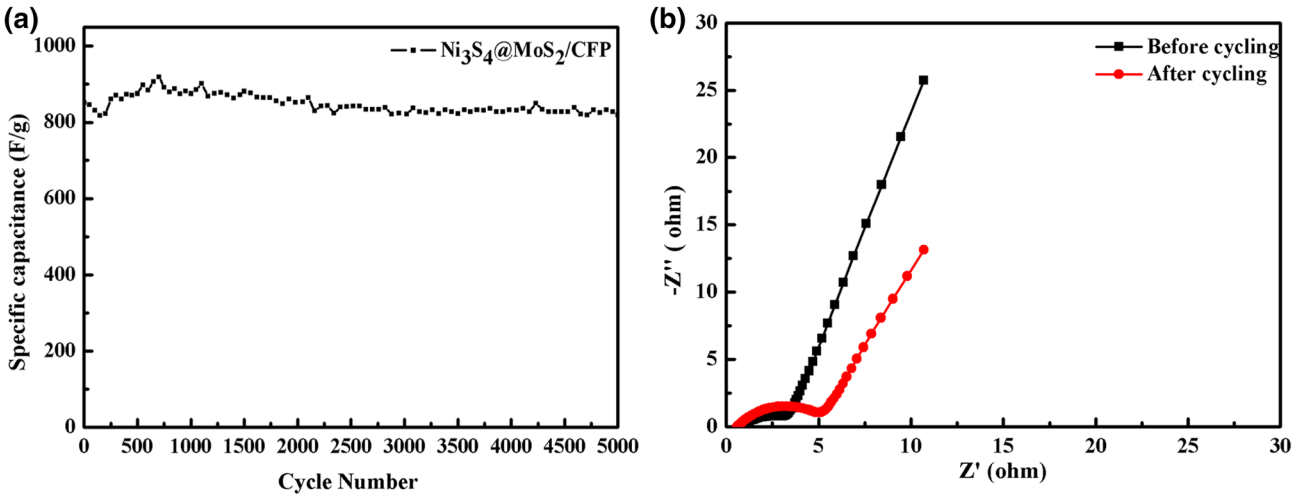

Fig. 6 **a** Cycling performance of Ni_3S_4@MoS_2/CFP at the current density of 5 A/g; **b** Nyquist plots of Ni_3S_4@MoS_2/CFP electrode in 2 M KOH solution in the frequency range from 0.01 to 100,000 Hz

promising and suitable electrode material for high-performance supercapacitors.

Acknowledgements The authors would like to acknowledge the support by the Fundamental Research Funds for the Central Universities (No. 2015QNA03).

References

1. P. Simon, Y. Gogotsi, Nat. Mater. **7**, 845 (2008)
2. M.D. Stoller, S. Park, Y. Zhu, J. An, R.S. Ruffo, Nano Lett. **8**, 3498 (2008)
3. L.L. Zhang, X.S. Zhao, Chem. Soc. Rev. **38**, 2520 (2009)
4. E. Frackowiak, Chem. Soc. Rev. **9**, 1774 (2007)
5. E. Frackowiak, K. Metenier, V. Bertagna, F. Beguin, Appl. Phys. Lett. **77**, 2421 (2000)
6. Q. Xiao, X. Zhou, Electrochim. Acta **48**, 575 (2003)
7. C.X. Guo, C.M. Li, Energy Environ. Sci. **4**, 4504 (2011)
8. Z. Huang, Z. Zhang, X. Qi, X. Ren, G. Xu, P. Wan, Nanoscale **8**, 13273 (2016)
9. X. Xia, J. Tu, Y. Zhang, X. Wang, C. Gu, X. Zhao, ACS Nano **6**, 5531 (2012)
10. M. Mastragostino, C. Arbizzani, F. Soavi, Solid State Ionics **148**, 493 (2002)
11. Y.T. Weng, N.L. Wu, J. Power Sources **238**, 69 (2013)
12. Z. Zhang, X. Liu, X. Qi, Z. Huang, L. Ren, J. Zhong, RSC Adv. **4**, 37278 (2014)
13. X. Rui, H. Tan, Q. Yan, Nanoscale **6**, 9889 (2014)
14. Z. Xing, Q. Chu, X. Ren, J. Tian, A.M. Asiri, K.A. Alamry, Electrochem. Commun. **32**, 9889 (2013)
15. C. Largeot, C. Portet, J. Chmiola, J. Am. Chem. Soc. **130**, 2730 (2008)
16. L. Cao, S. Yang, W. Gao, Z. Liu, Y. Gong, L. Ma, Small **9**, 2905 (2013)
17. A. Ramadoss, T. Kim, G.S. Kim, J.K. Sang, New. J. Chem. **38**, 2379 (2014)
18. L. Wang, M. Ying, Y. Min, Y. Qi, Electrochim. Acta **186**, 391 (2015)
19. X. Liu, X. Qi, Z. Zhang, L. Ren, Y. Liu, L. Meng, Ceram. Int. **40**, 8189 (2014)
20. S. Shen, Q. Wang, Cheminform **25**, 1166 (2012)
21. Z. Xing, Q. Chu, X. Ren, A.M. Asiri, K.A. Alamry, Electrochem. Commun. **32**, 9 (2013)
22. L. Wang, J. Liu, L.L. Zhang, B. Dai, M. Xu, M. Ji, RSC Adv. **5**, 8422 (2015)
23. Z. Zhang, Z. Huang, L. Ren, Y. Shen, Q.I. X., J. Zhong, Electrochim. Acta **149**, 316 (2014)
24. J. Yang, X. Duan, Q. Qin, W. Zheng, J. Mater. Chem. A **1**, 7880 (2013)
25. K.J. Huang, L. Wang, Y.J. Liu, Y.M. Liu, H.B. Wang, T. Gan, Int. J. Hydrog. Energy **38**, 14027 (2013)
26. L. Hou, C. Yuan, D. Li, L. Yang, L. Shen, F. Zhang, Electrochim. Acta **56**, 7454 (2011)
27. W. Wei, L. Mi, Y. Gao, Z. Zheng, W. Chen, X. Guan, Chem. Mater. **26**, 3418 (2014)
28. C. Yuan, B. Gao, L. Su, L. Chen, X. Zhang, J. Electrochem. Soc. **156**, A199 (2009)
29. Z. Zhang, Y. Liu, Z. Huang, L. Ren, X. Qi, X. Wei, Phys. Chem. Chem. Phys. **17**, 20795 (2015)